

Optical orientation and alignment of excitons in direct and indirect band gap (In,Al)As/AIAs quantum dots with type-I band alignment

J. Rautert,¹ T. S. Shamirzaev,^{2,3} S. V. Nekrasov,⁴ D. R. Yakovlev,^{1,4} P. Klenovský,^{5,6,7} Yu. G. Kusrayev,⁴ and M. Bayer^{1,4}

¹*Experimentelle Physik 2, Technische Universität Dortmund, 44227 Dortmund, Germany*

²*Rzhanov Institute of Semiconductor Physics, Siberian Branch of the Russian Academy of Sciences, 630090 Novosibirsk, Russia*

³*Ural Federal University, 620002 Yekaterinburg, Russia*

⁴*Ioffe Institute, Russian Academy of Sciences, 194021 St. Petersburg, Russia*

⁵*Department of Condensed Matter Physics, Faculty of Science, Masaryk University, Kotlářská 267/2, 61137 Brno, Czech Republic*

⁶*Central European Institute of Technology, Masaryk University, Kamenice 753/5, 62500 Brno, Czech Republic*

⁷*Czech Metrology Institute, Okružní 31, 63800 Brno, Czech Republic*



(Received 2 April 2019; published 8 May 2019)

The spin structure and spin dynamics of excitons in an ensemble of (In,Al)As/AIAs quantum dots (QDs) with type-I band alignment, containing both direct and indirect band gap dots, are studied. Time-resolved and spectral selective techniques are used to distinguish between the direct and indirect QDs. The exciton fine structure is studied by means of optical alignment and optical orientation techniques in magnetic fields applied in the Faraday or Voigt geometries. A drastic difference in emission polarization is found for the excitons in the direct QDs involving a Γ -valley electron and the excitons in the indirect QDs contributed by an X-valley electron. We show that in the direct QDs the exciton spin dynamics is controlled by the anisotropic exchange splitting, while in the indirect QDs it is determined by the hyperfine interaction with nuclear field fluctuations. The anisotropic exchange splitting is determined for the direct QD excitons and compared with model calculations.

DOI: [10.1103/PhysRevB.99.195411](https://doi.org/10.1103/PhysRevB.99.195411)

I. INTRODUCTION

Semiconductor quantum dots (QDs) have been studied for many years due to the broad range of optical applications that they offer [1,2]. One of the fundamental parameters of excitons confined in QDs is their recombination time that can be controlled by the type of band gap [3]. Recently, we have demonstrated the coexistence of both direct and indirect band gap QDs with type-I band alignment in a (In,Al)As/AIAs semiconductor heterosystem. This system demonstrates intensive luminescence up to room temperature [4] provided by the strong localization of electrons and holes in (In,Al)As QDs confined by AIAs barriers with a large band gap. Recombination dynamics of indirect excitons is extremely long extending up to several hundreds of microseconds at cryogenic temperatures, which allows one to study long living spin dynamics [5]. The difference of direct and indirect in momentum space excitons was manifested by different optical techniques: (i) time-resolved photoluminescence (PL) addressing the recombination dynamics [5,6], (ii) optically detected magnetic resonance [7], and (iii) spin-flip Raman scattering [8] via the g factors of the Γ and X valley electrons.

In this paper, we study the fine structure of the direct and indirect excitons in (In,Al)As/AIAs QDs with type-I band alignment. Time-resolved photoluminescence and luminescence after selective excitation allow us to distinguish QDs with direct and indirect band gap in momentum space, which are coexisting also in this QD ensemble [6]. The fine structure is determined via study of the polarization of photoluminescence. For the direct band gap QDs linearly-polarized

emission under resonant linearly-polarized excitation (optical alignment) and the absence of circularly-polarized emission under resonant circularly-polarized excitation (optical orientation) are found. However, for the indirect band gap QDs, unexpectedly, on one hand a negligible optical alignment and on the other hand pronounced optical orientation are revealed. The anisotropic electron-hole (e-h) exchange splitting (δ_1) of the excitons in the direct band gap QDs is determined. We also demonstrate that for the indirect band gap QDs the exciton spin relaxation time (T_1) considerably exceeds the exciton radiative recombination time, which is in the tens of microsecond range.

The paper is organized as follows. In Sec. II, the studied sample and used experimental techniques are described. In Sec. III the emission spectra of an ensemble of (In,Al)As/AIAs QDs with type-I band alignment, containing QDs with direct and indirect band gap, are investigated. Using nonresonant time-resolved and selectively excited time-integrated photoluminescence spectroscopy we uniquely determine the spectral features of the excitons confined in the direct and indirect band gap QDs. Optical alignment and optical orientation of the excitons is studied as a function of magnetic fields in Sec. IV. Model calculations of the exciton fine structure are given in Sec. V.

II. EXPERIMENTAL DETAILS

The studied structure (AG 2890) contains 20 layers of undoped (In,Al)As/AIAs QDs grown by molecular-beam epitaxy on a (001)-oriented GaAs substrate. The density of the lens-shaped QDs with an average diameter of 15 nm and a

height of 4 nm is about $3 \times 10^{10} \text{ cm}^{-2}$ in each layer. The QD layers are separated from each other by 20-nm-thick AlAs barriers, which prevent an electronic coupling between QDs in adjacent layers. A 20-nm-thick GaAs cap layer protects the top AlAs barrier against oxidation. The growth axis coincides with the crystallographic direction (001) and is defined as the z axis. Note that the band gap energy of the GaAs substrate is 1.52 eV and that of the AlAs barrier is 2.30 eV [9]. Further growth details are given in Ref. [10].

The sample was mounted either in a liquid helium bath cryostat or a cold-finger closed-cycle cryostat. The temperature was varied from $T = 1.6$ up to 50 K. In the studied QDs the intensity, energy position, and polarization degree of the exciton photoluminescence were about the same in the temperature range from 1.6 to 10 K. Low magnetic fields (in the mT range) were generated by an electromagnet and high magnetic fields (up to 10 T) by a superconducting split-coil solenoid. The magnetic field was applied either parallel to the structure growth axis ($\mathbf{B} \parallel z$) in the Faraday geometry or perpendicular to it ($\mathbf{B} \perp z$) in the Voigt geometry. The wave vector of the excitation light was always parallel to the structure growth axis.

The photoluminescence was excited either nonresonantly with the photon energy of the laser exceeding considerably the emission energies in the QD ensemble, or selectively with the laser energy tuned within the inhomogeneously broadened exciton emission band of QDs. The nonresonant excitation was provided by the third harmonic of a Q-switched Nd:YVO₄ pulsed laser with photon energy of 3.49 eV, a pulse duration of 5 ns and a repetition rate of $f = 2$ kHz. The excitation density was kept below 100 nJ/cm^2 [5].

For selective excitation two lasers were used: (i) an optical parametric oscillator with tunable photon energy in the spectral range from 1.5 to 2.0 eV, pulse duration of 1 ps extended by a multimode optical fiber up to 1 ns and repetition rate of $f = 2$ kHz; (ii) a tunable continuous-wave Ti:sapphire laser. Both techniques provide similar spectra of QDs, therefore, we do not specify the used excitation technique in the text.

The photoluminescence was dispersed by a 0.5 m monochromator. For the time-integrated measurements under nonresonant excitation the PL was detected by a liquid-nitrogen-cooled charge-coupled-device (CCD) camera. In order to avoid scattered light from the laser in experiments with selective excitation we used a gated CCD camera synchronized with the laser via an external trigger signal. For the time-resolved PL at nonresonant excitation, the time delay between laser pulse and the begin of recording, t_{delay} , was varied in the range from 1 ns up to 100 μs . The duration of recording, i.e., the gate window t_{gate} , was varied from 4 ns to 50 μs in order to optimize the signal intensity and the time resolution. The best time resolution of the detection system was 1 ns.

For measuring the optical alignment and optical orientation effects, linear or circular polarization of the excitation laser and of the PL were selected by linear and circular polarizers (Glan-Thompson prism, as well as quarter-wave and half-wave plates). For the optical alignment measurement, the linear polarization degree of the PL (ρ_l) induced under linearly polarized excitation is measured. The linear polarization

degree is defined as

$$\rho_l = \frac{I^{0/0} - I^{0/90}}{I^{0/0} + I^{0/90}}, \quad (1)$$

where $I^{a/b}$ are the PL intensities with the subscripts a/b corresponding to the direction of excitation/detection linear polarization. The direction “0” is parallel to the [110] crystallographic direction and the direction “90” is parallel to the $[\bar{1}\bar{1}0]$ direction. For the optical orientation measurement, the circular polarization degree of the PL induced by circularly-polarized excitation, ρ_c , is measured.

$$\rho_c = \frac{I^{+/+} - I^{+/-}}{I^{+/+} + I^{+/-}}. \quad (2)$$

Here $I^{a/b}$ is the intensity of the σ^b -polarized PL component measured after σ^a -polarized excitation. The labels + and – correspond to right-hand and left-hand circular polarization, respectively.

III. ENERGY SPECTRA OF QUANTUM DOTS

In this paper we study (In,Al)As/AlAs QDs with type-I band alignment, where the electrons and holes have their minimum energy in the (In,Al)As dots and therefore are confined there, see Fig. 1(b). For all QD sizes the hole is located in the center of the Brillouin zone. For large QDs the lowest electron state of the conduction band is in the Γ valley and, therefore, the band gap is direct in momentum space. In what follows, we will call these QDs the direct QDs. Contrary to that, in small QDs the quantum confinement shifts the Γ valley of the conduction band in energy above the X valley and the band gap becomes indirect in momentum space. We will specify these QDs as the indirect QDs. It was shown that due to inhomogeneous broadening an ensemble of (In,Al)As/AlAs QDs is composed of direct and indirect dots, whose emissions are partly overlapping [6–8,10]. As we will show below, the direct and indirect QDs can be well distinguished from each other by different optical techniques.

A. Time-resolved photoluminescence under nonresonant excitation

Photoluminescence spectra of an (In,Al)As/AlAs QD ensemble measured under nonresonant excitation are shown in Fig. 1(a). The time-integrated spectrum (black line) has a maximum at 1.80 eV and extends from 1.55 to 1.95 eV having a full width at half maximum (FWHM) of 200 meV. The large width of emission band is due to the dispersion of the QD parameters, since the exciton energy depends on the QD size, shape, and composition [10]. The PL band is contributed by the emission of direct and indirect QDs, which becomes evident from the time-resolved PL spectra. As they are measured immediately after the laser pulse application ($t_{\text{delay}} = 1$ ns and $t_{\text{gate}} = 4$ ns), the PL band has a maximum at 1.66 eV and a FWHM of 120 meV only (red line). For longer delays ($t_{\text{delay}} = 1000$ ns and $t_{\text{gate}} = 500$ ns), the emission shifts to 1.78 eV and broadens to 190 meV (blue line), rather similar to the time-integrated PL spectrum.

The strong modification of the time-resolved spectra is provided by the very different exciton recombination dynamics in

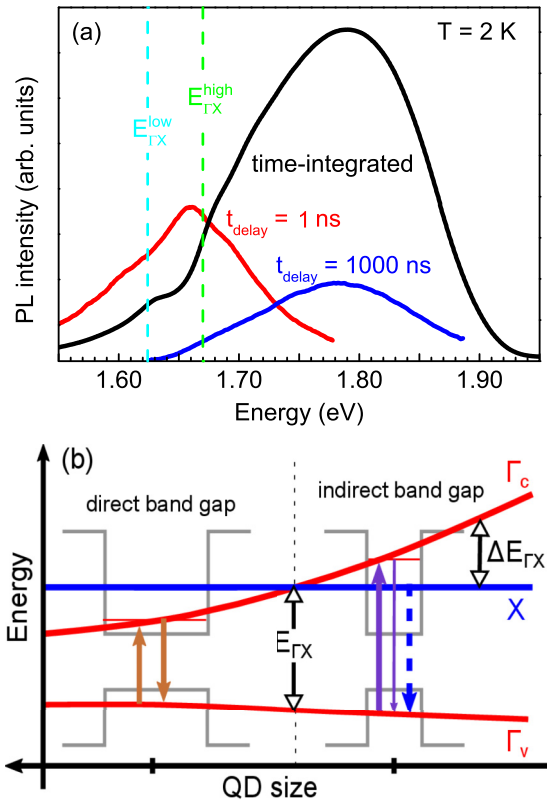


FIG. 1. (a) Photoluminescence spectra of (In,Al)As/AIAs QDs measured under nonresonant excitation: time-integrated (black line), time-resolved for $t_{\text{delay}} = 1$ ns and $t_{\text{gate}} = 4$ ns (red), and for $t_{\text{delay}} = 1000$ ns and $t_{\text{gate}} = 500$ ns (blue). Vertical dashed lines $E_{\Gamma X}^{\text{low}}$ (cyan) and $E_{\Gamma X}^{\text{high}}$ (green) mark ΓX -crossing energies, see Sec. III B. (b) Band structure schematics for two (In,Al)As/AIAs QDs of different sizes with either the Γ or the X valley as the lowest conduction band state. Vertical arrows mark the excitation and emission energies. Solid arrows correspond to direct in momentum space and dashed ones to indirect in momentum space optical transitions. Dashed vertical line $E_{\Gamma X}$ indicates the QD size with equal energies of the Γ and X electron levels. $\Delta E_{\Gamma X}$ is the splitting between the Γ and X electron levels in the conduction band.

direct and indirect QDs [5,6]. We have demonstrated recently that after the photoexcitation in the AIAs barriers electrons and holes are captured in QDs within several picoseconds, and the capture probability does not depend on the QD size and composition [11]. Therefore, all QDs in the ensemble (direct and indirect) become equally populated shortly after the excitation pulse. The exciton recombination dynamics is fast for direct QDs, for which emission occurs mainly in the spectral range of 1.50–1.78 eV. It is slow for the indirect QDs emitting in the 1.63–1.95 eV range. The emission of the direct and indirect QDs overlaps in the range of 1.63–1.78 eV. Here, for further clarification of the relative contributions of the two different types of QDs to the PL signal, the selective excitation techniques can be used.

B. Time-integrated photoluminescence under selective excitation

Selective excitation within an inhomogeneously broadened PL line is a common technique that allows one to excite only

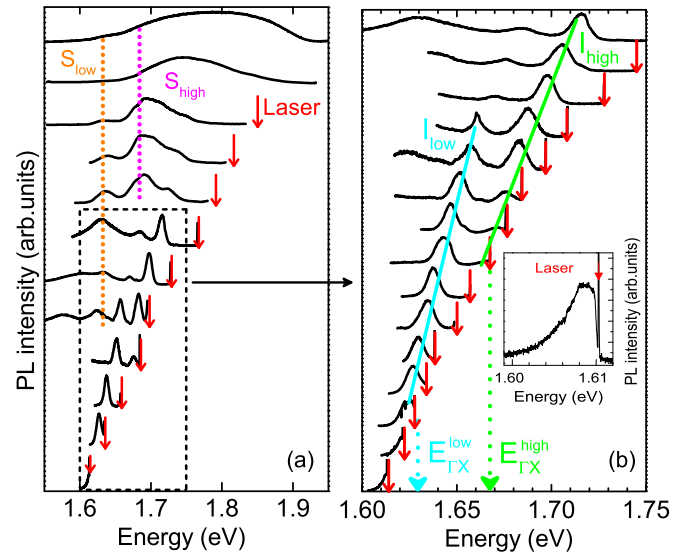


FIG. 2. (a) Photoluminescence spectra for different excitation energies indicated by the red arrows. $T = 2$ K. Dotted lines indicate the S_{low} and S_{high} PL lines that do not move with varying laser energy. (b) Closeup of the PL spectra from panel (a). Cyan and green lines trace the shifts of the I_{low} and I_{high} lines from indirect QDs. Crossing energies of the PL lines from the direct and indirect QDs are $E_{\Gamma X}^{\text{low}} = 1.63$ eV and $E_{\Gamma X}^{\text{high}} = 1.67$ eV, marked by the vertical dashed arrows. The inset shows the PL spectrum for $E_{\text{exc}} = 1.61$ eV energy excitation.

the fraction of QDs, whose direct exciton transition matches the laser energy E_{exc} . As a result, the PL band is transformed into a spectrum with narrow lines, which is known as fluorescence line narrowing. For example, in colloidal CdSe quantum dots such a narrowed PL spectrum consists of the lines of optically-allowed and optically-forbidden excitons and exciton recombination lines assisted by LO-phonon emission [12,13]. We will show below that this technique is well suited and informative also for the studied (In,Al)As/AIAs QDs.

Time-integrated PL spectra measured under selective excitation tuned in the range of $E_{\text{exc}} = 1.61$ –1.95 eV as well as under nonresonant excitation at $E_{\text{exc}} = 3.49$ eV (topmost curve) are shown in Fig. 2(a). Here, the laser energies are marked by the red arrows. Scattered light from the laser was excluded by using a gated CCD, see Sec. II.

The inset of Fig. 2(b) shows the PL spectrum for $E_{\text{exc}} = 1.61$ eV energy excitation. At this energy only the direct QDs are excited and the recombination energy of the direct exciton demonstrates a small Stokes shift (about 2 meV) from the laser photon energy, see the left scheme in Fig. 1(b).

Also lines with very small intensity shifted to lower energies by 30 and 50 meV appear (not shown). These lines can be associated with the LO-phonon-assisted recombination of excitons involving the LO phonons of InAs (30 meV) and AIAs (50 meV) [14].

When the excitation energy is increased above 1.63 eV, which is on the low-energy side of the emission of indirect QDs [see Fig. 1(a)], additional lines appear in the spectra. As one can see from Fig. 2, the number of these lines, their energy position, and intensity depend on the excitation energy. In

order to clarify their properties and origin, we present in Fig. 3 the peak energy and intensity dependences on the excitation energy for these lines. These dependencies can be divided into three groups:

(1) The D-line and its two low-energy satellites related to LO-photon-assisted recombination with LO_{InAs} and LO_{AlAs} form the first group. These lines follow the energy shift of the laser. They are associated with exciton recombination in direct QDs, as illustrated in the left part of Fig. 1(b) by the orange arrow, and recombination of excited Γ -electron based exciton in indirect QDs [the violet arrow on the right part of Fig. 1(b)]. With increasing E_{exc} the D-line intensity shows a small increase and then diminishes by two orders of magnitude up to the excitation energy of 1.75 eV, see Fig. 3(b). The main reason for that is the decrease of the direct QD fraction in the ensemble with decreasing QD size. Also, with increasing E_{exc} more photons are absorbed in the indirect QDs, reducing the excitation efficiency of the direct QDs. Note that the indirect and direct QDs have the same efficiency of light absorption since the absorption is provided by the direct in momentum space optical transition to the Γ valley of the conduction band, as shown by the thick orange and violet arrows in Fig. 1(b).

(2) The two lines I_{low} and I_{high} shifting to higher energies with increasing E_{exc} with a slope about twice smaller than that of the D line and the laser itself form the second group. They are split off from the D line at $E_{\Gamma X}^{\text{low}} = 1.63$ eV (for I_{low}) and $E_{\Gamma X}^{\text{high}} = 1.67$ eV (for I_{high}); see the dotted arrows in Fig. 2(b). The shifts of these lines with E_{exc} can be interpolated by linear functions that are shown by the lines of corresponding colors in Fig. 3:

$$E_{\text{low}} [\text{eV}] = 0.420 \times E_{\text{exc}} + 0.942, \quad (3)$$

$$E_{\text{high}} [\text{eV}] = 0.461 \times E_{\text{exc}} + 0.901. \quad (4)$$

I_{low} and I_{high} lines are provided by exciton recombination in the indirect QDs. These dots are excited resonantly via a direct in momentum space optical transition, see the thick violet arrow in the right part of Fig. 1(b). Their emission, shown by the dashed blue arrow, is shifted from the excitation energy by the energy difference between the Γ and the X valleys in the conduction band, $\Delta E_{\Gamma X}$, which increases with increasing E_{exc} . This dependence is shown for the I_{low} line by the symbols in Fig. 4 and is compared with the results of model calculations (the solid line) using the simple-band effective-mass approach described in Ref. [10], which takes into account strain, deformation potentials, and nonparabolicity of the electron dispersion [15]. In this calculation we also take into account dependencies of the Γ and X electron levels on the QD size and shape (obtained from microscopy data), alloy composition and its gradient across a QD (obtained from growth condition using nomogram from Ref. [10]). One sees excellent agreement between the experimental data and the calculations, which is remarkable as we do not use any fitting parameters. The intensities of I_{low} and I_{high} lines have nonmonotonic dependencies on the excitation energy, as shown in Fig. 3(c).

It is surprising to observe two emission lines related to the indirect QDs. We explain that by a bimodal distribution in

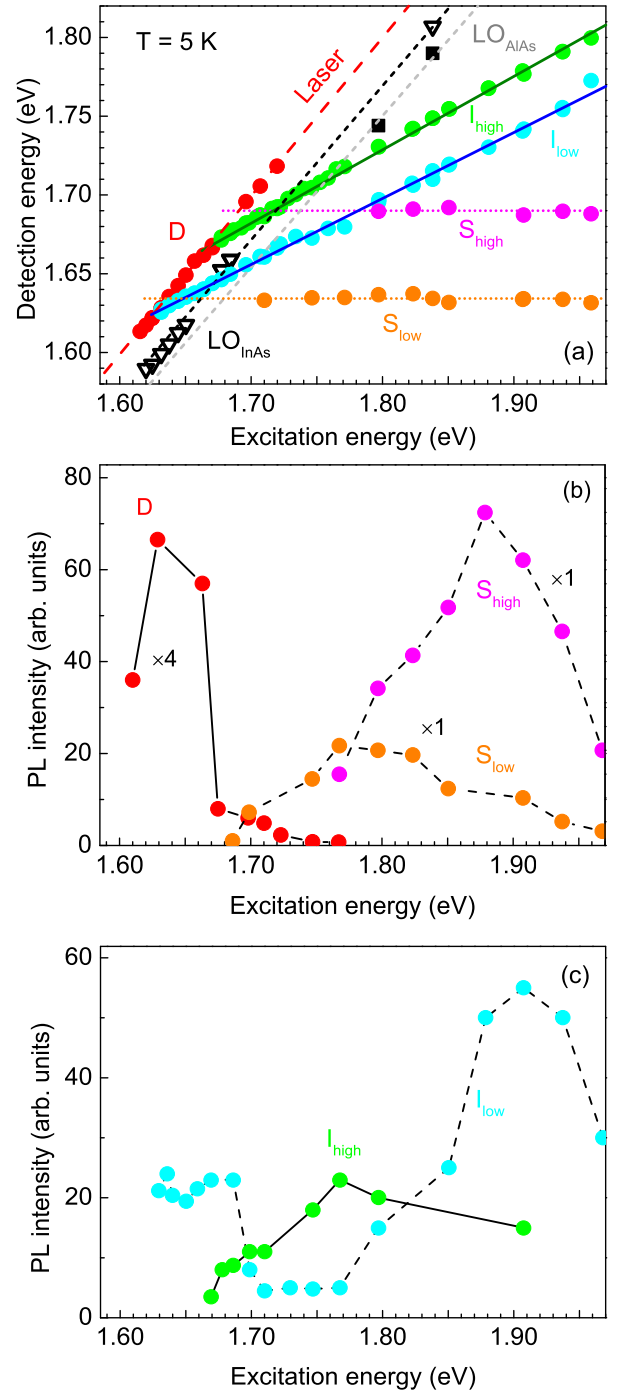


FIG. 3. Parameters of the PL lines in Fig. 2 plotted as a function of the excitation energy. (a) The shift of the laser is shown by the red line. Symbols give the energies of the PL lines: excitons in direct QDs (D-line, red dots); LO-photon-assisted emission from direct QDs: LO_{AlAs} (filled black squares), LO_{InAs} (open black triangles). Excitons in indirect QDs: low energy line (cyan dots) and high energy line (green dots); S_{low} (orange dots) and S_{high} (pink dots) PL lines that do not move with varying laser energy. Dashed and dotted lines are guides for the eye. Solid lines are fits using Eqs. (3) and (4) (see text). (b) Excitation energy dependencies of the intensity of the D-line (red dots), as well as the S_{low} (orange dots) and S_{high} (magenta dots) PL lines. Lines are guides for the eye. (c) Excitation energy dependencies of the I_{low} (cyan dots) and I_{high} (green dots) PL lines. Lines are guides for an eye.

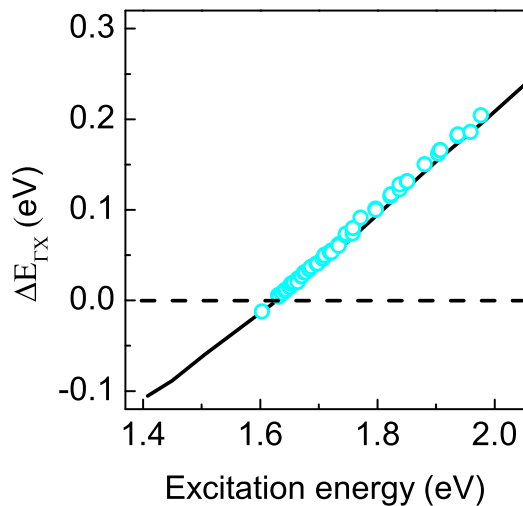


FIG. 4. Energy difference between the laser photon energy and the maximum of the I_{low} line presented as a function of E_{exc} (the symbols). The calculated dependence of $\Delta E_{\Gamma X}$ in (In,Al)As/AlAs QDs versus excitation energy is shown by the solid line. The dashed line gives the zero level.

the QD ensemble. Possibly the studied sample contains two subensembles of QDs with different shape and/or composition. Each of them is characterized by its own $E_{\Gamma X}$. The reason for such a bimodal distribution is still not clarified, most probably it is determined by the sample growth conditions.

Let us discuss the role of the direct emission from the indirect QDs. After resonant excitation through the direct optical transition, the direct exciton contributes to the emission at the laser photon energy. However, at liquid helium temperatures this state is quickly depopulated by electron relaxation to the X valley. We showed that the time of this relaxation is much shorter than the radiative recombination time of the direct exciton [11]. However, at elevated temperatures, when the Γ valley becomes thermally populated, observation of the direct emission from the indirect QDs is possible. In Figs. 5(b) and 5(c) one sees a redistribution of the emission intensity from the indirect to the direct recombination channel when a temperature is increased. The latter forms the low-energy

wing close to the excitation energy. For comparison, we show in Fig. 5(a) the temperature evolution of the D line in the direct QDs. Here only a decrease of the PL intensity is observed with raising temperature which is explained by the opening of nonradiative decay channels.

(3) The two lines S_{low} and S_{high} , which energies do not depend on the excitation energy [Figs. 2(a) and 3(a)], are in the third group. They are relatively broad lines. The S_{low} line has the peak energy at 1.635 eV and appears in the spectra for excitation energies exceeding 1.70 eV. The S_{high} line has the peak energy at 1.690 eV and appears for $E_{\text{exc}} > 1.80$ eV. The dependencies of their intensities on the excitation energy are shown in Fig. 3(b).

These lines show up in the time-integrated spectrum [Fig. 1(a)] in the spectral range corresponding to the ΓX transition for the I_{low} and I_{high} lines. The origin of the S_{low} and S_{high} lines is still unknown and is beyond the scope of this study.

IV. OPTICAL ALIGNMENT AND OPTICAL ORIENTATION

We have shown in Sec. III that the D, I_{low} , and I_{high} PL lines can be identified with excitons in direct and indirect QDs. This opens a way to study and compare the fine structures of these excitons using selective excitation together with optical alignment and optical orientation.

Note that for small values of $\Delta E_{\Gamma X}$ an admixing of Γ and X -electron states takes place [8]. However, the effect of this admixing on the exciton fine structure is not in the focus of this paper.

A. Direct and indirect QDs in zero magnetic field

Let us start with experiments performed at zero magnetic field. We choose two particular excitation energies to address either direct ($E_{\text{exc}} = 1.61$ eV) or indirect ($E_{\text{exc}} = 1.70$ eV) QDs and measure the respective optical alignment and optical orientation. Results for polarized PL spectra are shown in the four upper panels of Fig. 6. One can see that the properties of the direct and indirect QDs are very different with respect to optical alignment and orientation. In the direct QDs 53% of linearly polarization of PL is detected in the case of linear

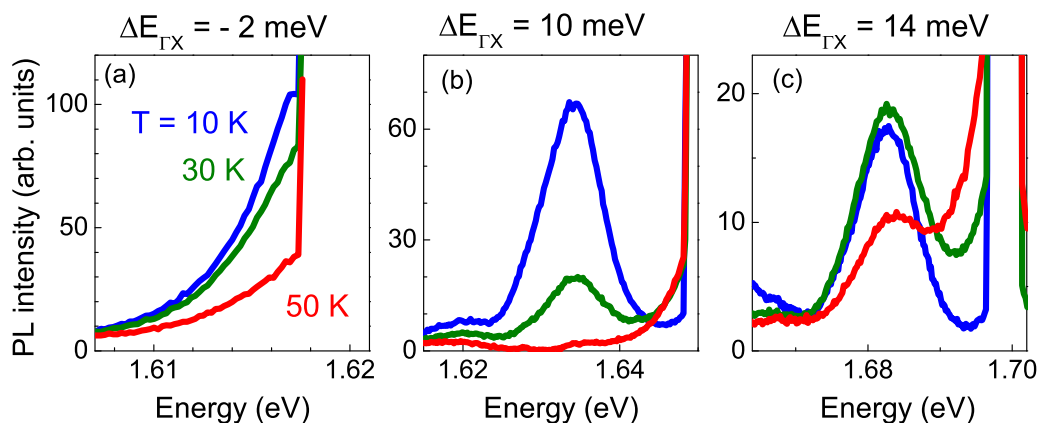


FIG. 5. Evolution of PL spectra with increasing temperature for (a) D line at $E_{\text{exc}} = 1.619$ eV, (b) I_{low} line at $E_{\text{exc}} = 1.645$ eV, and (c) I_{high} line at $E_{\text{exc}} = 1.696$ eV.

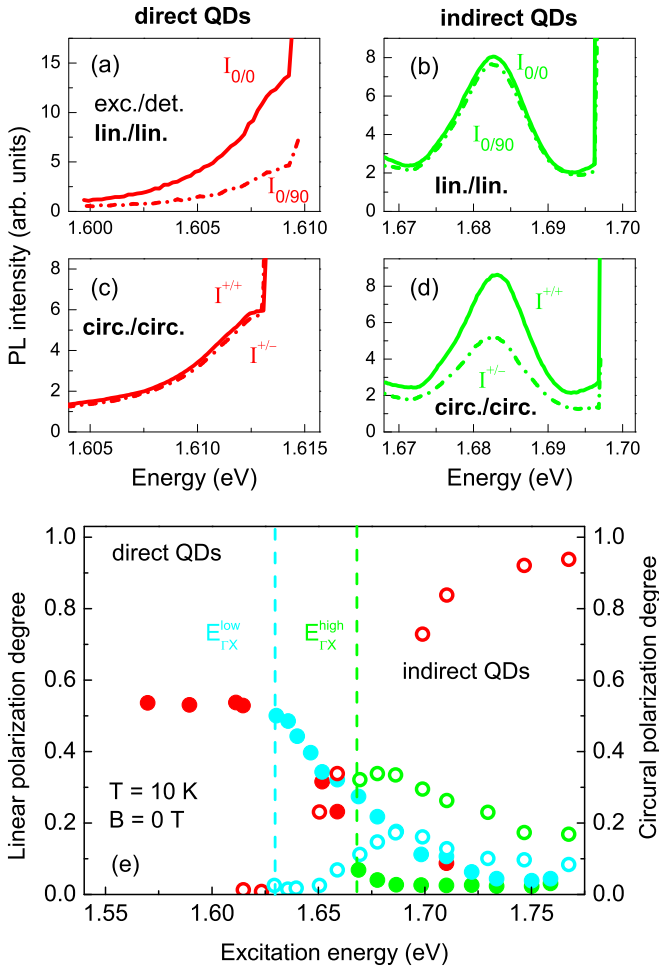


FIG. 6. Linear polarized PL intensities of direct (a) and indirect (b) excitons under linear polarized excitation. Circular polarized PL intensities of direct (c) and indirect (d) excitons under circular polarized excitation. $E_{\text{exc}} = 1.61 \text{ eV}$ for the direct QDs and $E_{\text{exc}} = 1.70 \text{ eV}$ for the indirect QDs. $T = 10 \text{ K}$. (e) Linear (filled circles) and circular (open circles) polarization degree of the emission for optical alignment and orientation, respectively, measured for the direct (D line, red symbols) and indirect excitons (lines I_{low} and I_{high} , cyan and green symbols, respectively) as a function of excitation energy. Vertical dashed lines $E_{\Gamma X}^{\text{low}}$ (cyan) and $E_{\Gamma X}^{\text{high}}$ (green) mark ΓX -crossing energies, see Sec. III B.

polarized excitation, while the circular polarization in the case of circular polarized excitation is negligible, compare Figs. 6(a) and 6(c). Contrary to that, in the indirect QDs the optical alignment does not exceed 2%, but the optical orientation reaches 33%, Figs. 6(b) and 6(d).

These results can be explained by considering the exciton fine structure. It is known that for axial symmetrical QDs the exciton states are fourfold degenerate in the case of (hypothetical) absence of the electron-hole exchange interaction. A nonzero isotropic exchange interaction splits the exciton state, which is characterized by the total angular momentum projections $J_z = \pm 1, \pm 2$, into the doubly-degenerate bright and doubly-degenerate dark exciton states with $J_z = \pm 1$ and $J_z = \pm 2$, respectively. The breaking of the axial symmetry in real QDs lifts the degeneracy of the bright exciton states

and mixes them so that the following states emerge: $|X\rangle = \frac{1}{\sqrt{2}}(|+1\rangle + |-1\rangle)$ and $|Y\rangle = \frac{1}{i\sqrt{2}}(|+1\rangle - |-1\rangle)$ [16].

A circular polarized photon excites the superposition states $|X\rangle$ and $|Y\rangle$, which coherence is rapidly lost with time [17]. The decoherence time equals \hbar/δ_1 , where δ_1 is the splitting of the $|X\rangle$ and $|Y\rangle$ doublet by the anisotropic part of the electron-hole exchange interaction. If the decoherence time is much shorter than the exciton recombination time, τ_R , the optical orientation of the excitons is destroyed. In contrast to circular polarized light, linear polarized photons excite the pure states $|X\rangle$ and $|Y\rangle$ of the direct exciton, so that the linear polarization degree of the emission (optical alignment) is controlled by the ratio of the exciton spin relaxation time to τ_R . The high value of more than 50% of optical alignment shown for the direct QDs in Fig. 6(a) leads us to the conclusion that the spin relaxation time exceeds the recombination one, which is typical for the direct band gap QDs [17].

In indirect QDs the exchange interaction is weak because the wave functions of the X electron and the Γ hole overlap weakly in momentum space [18,19]. Thus, the mixing of the electron spin states is decreased and the pure exciton spin states $|\pm 1\rangle$ are formed. Therefore, in the indirect QDs with small or absent anisotropic exchange splitting δ_1 , a larger circular polarization degree can be realized. This is in line with our experimental data presented in Fig. 6(d).

We have performed a detailed study of the spectral dependence of the optical alignment and optical orientation in the range of excitation energies from 1.57 to 1.77 eV. The results for the direct (D-line) and indirect (I_{low} and I_{high} lines) excitons are summarized in Fig. 6(e).

The optical alignment of the D line (direct exciton, marked by red solid circles) has a plateau of $\rho_1 = 53\%$ in the range of $E_{\text{exc}} = 1.57\text{--}1.61 \text{ eV}$. Near the crossing energy $E_{\Gamma X}^{\text{low}}$ the ρ_1 starts to decrease.

In indirect QDs the optical alignment is also strongly dependent on the excitation energy. The low-energy indirect exciton (I_{low} line, solid cyan circles) has $\rho_1 = 50\%$ at the crossing energy $E_{\Gamma X}^{\text{low}}$, which is the same as for the D line in the direct QDs, compare the solid cyan and red circles in Fig. 6(e). For larger E_{exc} the linear polarization degree decreases monotonically down to a constant level of $\rho_1 = 2\%$ for excitation energies exceeding 1.75 eV. The second indirect optical transition (I_{high} line, solid green circles) has $\rho_1 = 6\%$ at its appearance energy $E_{\Gamma X}^{\text{high}}$, which quickly decreases down to 2% for $E_{\text{exc}} > 1.69 \text{ eV}$.

Let us turn to the spectral dependence of the optical orientation shown by the open circles in Fig. 6(e). For the D line (red) it is zero for $E_{\text{exc}} \leq 1.62 \text{ eV}$. Its increase starts at $E_{\Gamma X}^{\text{low}}$ with the transition from direct to indirect QDs and ρ_c reaches 95% at $E_{\text{exc}} > 1.75 \text{ eV}$. Note, that the increase in ρ_c is correlated with the decrease of the D-line intensity, Fig. 3(b). Both dependences arise from the decreasing lifetime of the direct exciton in indirect QDs, as discussed in Sec. III B, which is controlled by its fast scattering into the indirect exciton state. The optical orientation degree ρ_c is determined by the ratio of the exciton spin relaxation time to its lifetime. In direct QDs the exciton lifetime, being controlled by the radiative recombination, is longer than the decoherence time τ_d , which is inversely proportional to \hbar/δ_1 , so that circular

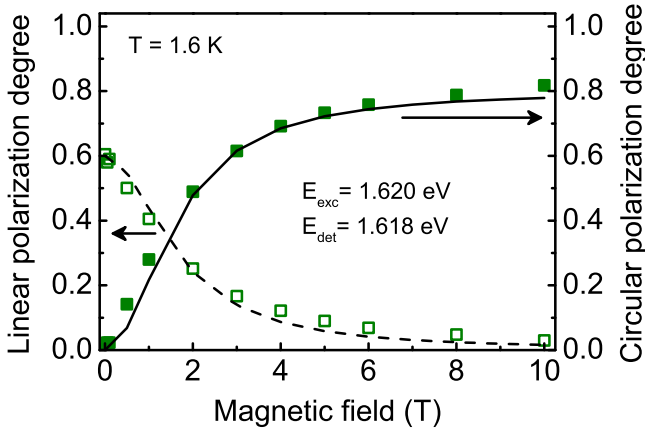


FIG. 7. Degree of linear (open square) and circular (filled square) polarization of the direct exciton emission (D line) as a function of longitudinal magnetic field (Faraday geometry). Lines show fits to experimental data with Eqs. (5) and (6) using the single fitting parameter $\delta_1 = 260 \pm 10 \mu\text{eV}$.

polarization during the exciton lifetime disappears and $\rho_c \approx 0$. However, in indirect QDs the lifetime of the direct excitons becomes very short, which provides a revival of the large optical orientation observed even in QDs with considerable anisotropic exchange splitting δ_1 of the direct exciton, which is not the ground state in the indirect dots.

The optical orientation of the indirect excitons in the indirect QDs is shown in Fig. 6(e) by the cyan and green open circles for the I_{low} and I_{high} lines, respectively. The circular polarization degree of the I_{low} increases with growing E_{exc} and reaches $\rho_c = 17\%$ at 1.68 eV. It shows a decrease down to 9% with further rise of the excitation energy. The I_{high} line reaches its maximum optical orientation of 33% at 1.675 eV, i.e., shortly above the appearance of this line at $E_{\Gamma X}^{\text{high}}$. Then it decreases down to 17% for the excitation energy reaching 1.77 eV. This decrease can be explained by an enhanced depolarization of the excitons caused by their scattering from the direct to the indirect state, i.e., by the electron scattering from the Γ to X valley before exciton recombination. The energy dissipated by this scattering equals to $\Delta E_{\Gamma X}$. It increases for smaller QDs requiring, e.g., more acoustic phonons, which in turn enhances the perturbation of the exciton spins.

B. Effect of the magnetic field on optical alignment and orientation in direct QDs

The application of magnetic field is a powerful tool for the investigation of the exciton fine structure. The results on optical alignment and optical orientation in strong magnetic fields up to 10 T are shown in Fig. 7. Here the direct QDs were excited at $E_{\text{exc}} = 1.620$ eV. The magnetic field was applied in Faraday geometry ($\mathbf{B} \parallel z$). One sees that the optical alignment is suppressed by the magnetic field, as the linear polarization degree decreases from $\rho_l = 59\%$ at zero field down to 2% for $B = 10$ T. On the other hand, the optical orientation, which is absent at zero field, increases with increasing field and saturates at $\rho_c = 80\%$.

These experimental data are in good agreement with the theory. It was demonstrated in Ref. [20] that the longitudinal magnetic field suppresses the exciton spin alignment and restores the exciton spin orientation. These effects occur when the Zeeman splitting between the $|+1\rangle$ and $|-1\rangle$ exciton states exceeds the energy of the anisotropic exchange interaction δ_1 , which mixes these states. The magnetic field dependences of the linear and circular polarization degrees can be described by the following equations:

$$\rho_l(B) = \rho_l^0 \frac{\delta_1^2}{\delta_1^2 + (\mu_B g_{\text{ex}} B)^2}, \quad (5)$$

$$\rho_c(B) = \rho_c^{\text{max}} \frac{(\mu_B g_{\text{ex}} B)^2}{\delta_1^2 + (\mu_B g_{\text{ex}} B)^2}, \quad (6)$$

where ρ_l^0 is the linear polarization degree at zero magnetic field, and ρ_c^{max} is the maximal circular polarization degree achieved in strong fields, μ_B is the Bohr magneton, and g_{ex} is the longitudinal exciton g factor. The latter is composed of the Γ -electron (g_e) and heavy hole (g_{hh}) g factors: $g_{\text{ex}} = g_{\text{hh}} - g_e$. Both dependencies of $\rho_l(B)$ and $\rho_c(B)$ given by Eqs. (5) and (6) have a Lorentz shape and the same FWHM of $B_{1/2} = 2\delta_1/\mu_B g_{\text{ex}}$. We fit the experimental data for the direct QDs with Eqs. (5) and (6), see the lines in Fig. 7. The exciton g factor is $g_{\text{ex}} = 2.63$, as evaluated from the known values for $g_{\text{hh}} = 2.43$ [8] and $g_e = -0.2$ [21]. The only free parameter in the fit was δ_1 , which allows us to determine it to $\delta_1 = 260 \pm 10 \mu\text{eV}$, corresponding to $B_{1/2} = 3.1 \pm 0.15$ T. We theoretically confirm the value of the anisotropic exchange energy δ_1 and show that it agrees with calculations in Sec. V.

C. Effect of the magnetic field on the optical orientation in indirect QDs

Here we focus on the optical orientation of the indirect excitons in the indirect QDs. We choose $E_{\text{exc}} = 1.698$ eV and focus on the I_{high} line with maximum at 1.683 eV. For this line the optical alignment is absent and the optical orientation degree at zero magnetic field is $\rho_c = 33\%$. $\rho_c(B)$ demonstrates strong changes already in weak magnetic fields of a few mT and the changes depend on the field orientation, see Fig. 8.

For the Voigt orientation of the magnetic field ($\mathbf{B} \perp z$) the Hanle effect on the optical orientation is observed. Namely, the circular polarization degree is reduced down to zero with growing field. This decrease is well described by a Lorentz curve with a FWHM of 3.2 mT. When the magnetic field is applied in Faraday geometry ($\mathbf{B} \parallel z$), an increase of the circular polarization degree up to 89% takes place. This dependence can also be described by a Lorentz curve with FWHM of 3.8 mT, which in fact coincides with the width of the Hanle curve. Note that in the Faraday geometry the minimum of $\rho_c(B)$ is slightly shifted by -0.45 mT from the zero field value. We explain that by dynamic nuclear polarization [22].

The experimentally observed specifics of the optical orientation in indirect QDs presented in Fig. 8 are characteristic for the electron spin dynamics in QDs controlled by frozen nuclear spin fluctuations [23,24]. It is expected that in this case the widths of the Hanle curve and polarization recovery curve coincide. Also, the polarization recovery in Faraday geometry increases the polarization degree by a factor of

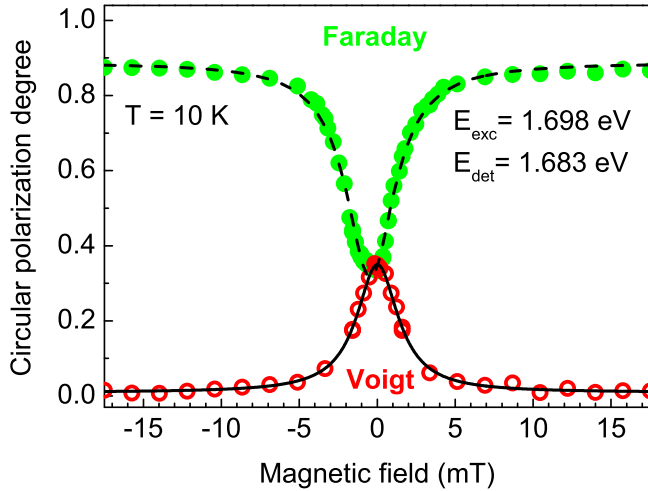


FIG. 8. Circular polarization degree of the I_{high} line as a function of magnetic field in Faraday (green filled circles) and Voigt (red open circles) geometry that are referred to in the text as polarization recovery curve and Hanle curve, respectively. Solid and dashed lines are fits by Lorentz curves with FWHMs of 3.2 and 3.8 mT, respectively.

3 being in line with model predictions. Note that the model considerations of Refs. [23,24] are formulated for an electron confined in a QD, but they can be readily used for our case of an electron in an indirect exciton, as for the X electron the exchange interaction with Γ hole is very weak and can be neglected [18,19].

The finite number of nuclear spins in a QD results in nuclear spin fluctuations. Their spin dynamics is very slow compared to the electron spin dynamics and, therefore, for the electron these fluctuations can be considered as frozen effective magnetic fields \mathbf{B}_N . The electron spin undergoes Larmor precession around \mathbf{B}_N with a frequency $\Omega_N = \mu_B g_e \mathbf{B}_N / \hbar$. If the condition $\Omega_N \tau_c \gg 1$ is valid, where τ_c is correlation time in the fluctuating magnetic fields, then the photogenerated 100% spin-oriented electrons lose 2/3 of their spin polarization as \mathbf{B}_N has no preferable spin orientation and its direction vary from dots to dots. The rest 1/3 of the electron polarization is stabilized via interaction with the nuclear spins pointing along the orientation direction that results in a PL polarization degree of about 33%. In experiment, the transverse magnetic field in Voigt geometry decreases this spin polarization. In this case it is in competition with the stabilization action of \mathbf{B}_N longitudinal component. As a result, $B_{1/2}$ of the Hanle curve should be equal to B_N . The longitudinal magnetic field in Faraday geometry stabilizes the 2/3 of the electron polarization that would be destructed by \mathbf{B}_N transverse component at zero field. In this case the field is again in competition with the nuclear fluctuations and $B_{1/2} = B_N$. It is worth noting that the spin polarization recovers to the very high value of 89%, which means that in magnetic fields exceeding 6 mT (Faraday geometry) the exciton spin relaxation time is considerably longer than the lifetime of the indirect exciton (up to 30 μs , that corresponds to the maximum of the radiative exciton recombination times distribution in the QD ensemble found by technique proposed in Ref. [5]).

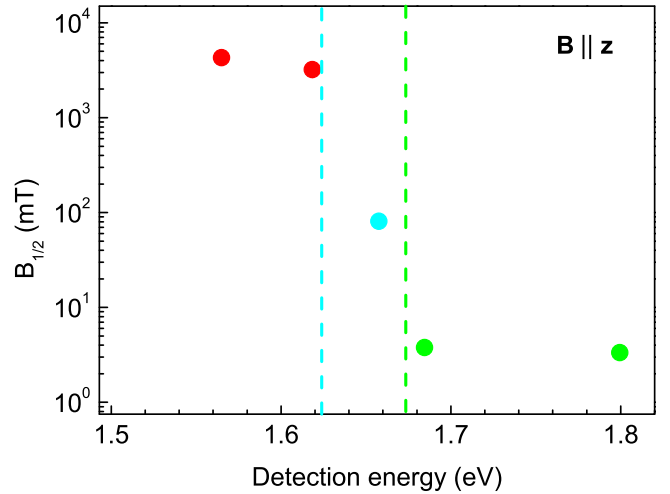


FIG. 9. Width $B_{1/2}$ of the longitudinal magnetic field dependencies of the circular polarization degree (Faraday geometry) measured in the direct QDs (D-line, red dot), and the indirect QDs (I_{low} and I_{high} lines, cyan and green dots, respectively). Vertical dashed lines $E_{\Gamma X}^{\text{low}}$ (cyan) and $E_{\Gamma X}^{\text{high}}$ (green) mark ΓX -crossing energies, see Sec. III B.

One also notes that by comparing the data from Figs. 7 and 8, the characteristic $B_{1/2}$ values differ by about three orders of magnitude for the excitons in the direct and indirect QDs. In Fig. 9 we plot the dependence of $B_{1/2}$ on the excitation energy. One can see that similar to other properties, like spectral shifts and polarizations, there are distinct spectral ranges for the direct and indirect QDs.

V. CALCULATION OF ANISOTROPIC EXCHANGE ENERGY

The exciton states in the (In,Al)As/AlAs direct quantum dots were calculated by computing the single particle states using the envelope function approximation based on the 8-band $\mathbf{k} \cdot \mathbf{p}$ method for both electrons and holes, using the nextnano++ simulation suite [25]. The obtained wave functions were then utilized as basis states for the configuration interaction (CI) method that takes into account the corrections due to the direct and exchange Coulomb interaction. The whole method is detailed in Ref. [26]. We consider here the exchange interaction up to second order of the multipole expansion [27,28]. Following Ref. [27] we mark the terms of that expansion as follows: monopole-monopole (EX_0), monopole-dipole (EX_1), and dipole-dipole (EX_2). The theoretical results of δ_1 for different sizes and shapes of QD with mean In content of 0.7 are shown in Fig. 10. Clearly, Fig. 10 shows that our calculations to a good approximation reproduce the experimental value of δ_1 deduced from fitting of the experimental data by Eqs. (5) and (6). Moreover, our calculations confirm the assumption that δ_1 depends on QD asymmetry (note e.g., the larger values of δ_1 for an alloy gradient compared to the constant In value in Fig. 10).

Finally we note that the magnitude of the anisotropic exchange interaction in indirect QDs is at least smaller than $\delta_{\text{max}} = \frac{1}{2} B_N \mu_B g_{\text{ex}}$, otherwise, the optical orientation in these QDs will be destroyed by the mixing of exciton states. Taking into account that $B_{1/2}$ of the Hanle curve should be equal to

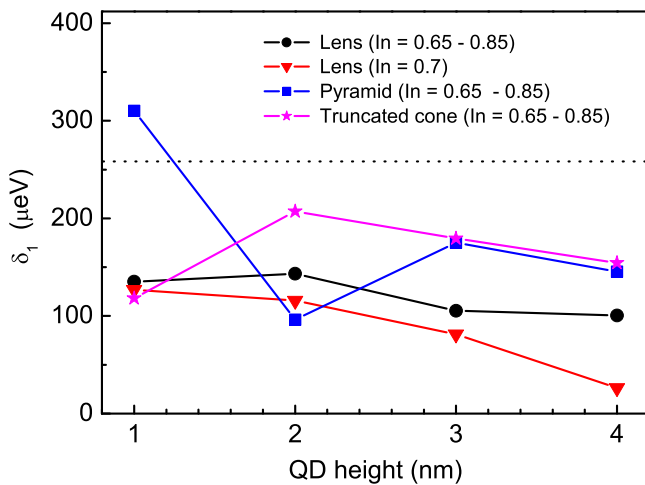


FIG. 10. Calculation of δ_1 for the direct exciton in (In,Al)GaAs/AlAs QD as a function of QD height for lens, pyramid, and truncated cone shaped QDs with an In content either of 0.7 set constant in the whole QD volume or linearly increasing along the dot vertical symmetry axis from 0.65 at QD base to 0.85 at QD apex. In all cases the QD base diameter was fixed to 15 nm. The data include $EX_0+EX_1+EX_2$ contributions in the exchange interaction, see text for details. The dotted horizontal line marks the value of $\delta_1 = 260 \mu\text{eV}$ obtained from fitting of the experimental data.

B_N and g_{ex} for indirect exciton in (In,Al)As/AlAs QDs equals to 0.43 [8] we can estimate the upper limit of the exchange splitting for an exciton in indirect QDs as $\delta_{\text{max}} = 4 \times 10^{-8} \text{ eV}$.

VI. CONCLUSIONS

The energy spectra and exciton fine structure in an (In,Al)As/AlAs QD ensemble with type-I band alignment with direct and indirect band gap have been investigated. Exciton optical alignment (orientation) was observed for

direct (indirect) band gap QDs. The anisotropic e-h exchange energy δ_1 for excitons in direct band gap QDs has been measured. The circular polarization degree for exciton emission after optical orientation in indirect band gap QDs is determined by the precession of the electron spin in the effective magnetic field of the nuclear spin frozen fluctuations. The effect of this hyperfine field of the frozen fluctuation of the nuclear spins on the circular polarization degree is overcome by a longitudinal field of 6 mT, resulting in $\rho_c = 89\%$. The large ρ_c value shows that the exciton spin relaxation time T_1 is much longer than the exciton radiative recombination time τ_R , which exceeds 30 μs .

ACKNOWLEDGMENTS

The authors are grateful to D. Dunker and J. Debus for their contribution in initial stages of this work. This work was supported by the Deutsche Forschungsgemeinschaft via the Project No. 409810106 and in the frame of the International Collaborative Research Center TRR 160 (Projects A1, B2 and B4), by the Russian Foundation for Basic Research (Grants No. 19-02-00098 and No. 19-52-12001), by the Government of the Russian Federation Grant No. 14.Z50.31.0021 (leading scientist M.B.), and by Act 211 Government of the Russian Federation (Contract No. AAAA-A17-117042110141-5). Yu.G.K. and N.S.V. thank the Russian Science Foundation for support of the experimental studies performed in the Ioffe Institute via Grant No. 18-12-00352. P.K. acknowledges the support of his theory studies by the national funding from the MEYS and the funding from European Union's Horizon 2020 (2014-2020) research and innovation framework programme under Grant Agreement No. 731473 and by project EMPIR 17FUN06 SIQUEST. This project received funding from the EMPIR programme co-financed by the Participating States and from the European Union Horizon 2020 research and innovation programme.

- [1] *Semiconductor Quantum Bits*, edited by F. Henneberger and O. Benson (Pan Stanford, Singapore, 2008).
- [2] *Optical Generation and Control of Quantum Coherence in Semiconductor Nanostructures*, edited by G. Slavcheva and P. Roussignol (Springer-Verlag, Berlin, 2010).
- [3] T. S. Shamirzaev, J. Debus, D. R. Yakovlev, M. M. Glazov, E. L. Ivchenko, and M. Bayer, Dynamics of exciton recombination in strong magnetic fields in ultrathin GaAs/AlAs quantum wells with indirect band gap and type-II band alignment, *Phys. Rev. B* **94**, 045411 (2016).
- [4] T. S. Shamirzaev, A. M. Gilinsky, A. K. Bakarov, A. I. Toropov, D. A. Tenne, K. S. Zhuravlev, C. von Borczyskowski, and D. R. T. Zahn, Millisecond photoluminescence kinetics in a system of direct-bandgap InAs quantum dots in an AlAs matrix, *Pis'ma v Zh. Eksp. Teor. Fiz.* **77**, 459 (2003) [*JETP Lett.* **77**, 389 (2003)].
- [5] T. S. Shamirzaev, J. Debus, D. S. Abramkin, D. Dunker, D. R. Yakovlev, D. V. Dmitriev, A. K. Gutakovskii, L. S. Braginsky, K. S. Zhuravlev, and M. Bayer, Exciton recombination

dynamics in an ensemble of (In, Al)As/AlAs quantum dots with indirect band-gap and type-I band alignment, *Phys. Rev. B* **84**, 155318 (2011).

- [6] T. S. Shamirzaev, A. V. Nenashev, and K. S. Zhuravlev, Coexistence of direct and indirect band structures in arrays of InAs/AlAs quantum dots, *Appl. Phys. Lett.* **92**, 213101 (2008).
- [7] V. Yu. Ivanov, T. S. Shamirzaev, D. R. Yakovlev, A. K. Gutakovskii, Ł. Owczarczyk, and M. Bayer, Optically detected magnetic resonance of photoexcited electrons in (In, Al)As/AlAs quantum dots with indirect band gap and type-I band alignment, *Phys. Rev. B* **97**, 245306 (2018).
- [8] J. Debus, T. S. Shamirzaev, D. Dunker, V. F. Sapega, E. L. Ivchenko, D. R. Yakovlev, A. I. Toropov, and M. Bayer, Spin-flip Raman scattering of the Γ -X mixed exciton in indirect band gap (In, Al)As/AlAs quantum dots, *Phys. Rev. B* **90**, 125431 (2014).
- [9] I. Vurgaftman, J. R. Meyer, and L. R. Ram-Mohan, Band parameters for III-V compound semiconductors and their alloys, *J. Appl. Phys.* **89**, 5815 (2001).

- [10] T. S. Shamirzaev, A. V. Nenashev, A. K. Gutakovskii, A. K. Kalagin, and K. S. Zhuravlev, Atomic and energy structure of InAs/AlAs quantum dots, *Phys. Rev. B* **78**, 085323 (2008).
- [11] T. S. Shamirzaev, D. S. Abramkin, A. V. Nenashev, K. S. Zhuravlev, F. Trojanek, B. Dzurak, and P. Maly, Carrier dynamics in InAs/AlAs quantum dots: lack in carrier transfer from wetting layer to quantum dots, *Nanotechnology* **21**, 155703-7 (2010).
- [12] M. Nirmal, D. J. Norris, M. Kuno, M. G. Bawendi, A. L. Efros, and M. Rosen, Observation of the Dark Exciton in CdSe Quantum Dots, *Phys. Rev. Lett.* **75**, 3728 (1995).
- [13] L. Biadala, E. V. Shornikova, A. V. Rodina, D. R. Yakovlev, B. Siebers, T. Aubert, M. Nasilowski, Z. Hens, B. Dubertret, A. L. Efros, and M. Bayer, Magnetic polaron on dangling-bond spins in CdSe colloidal nanocrystals, *Nat. Nanotech.* **12**, 569 (2017).
- [14] *Physics of Group IV Elements and III-V Compounds*, edited by O. Madelung, M. Schulz, and H. Weiss, Landolt-Börnstein Numerical Data and Relationships, New Series, Group III, Vol. 17, Part A (Springer, Berlin, 1982).
- [15] O. E. Kane, Band structure of indium antimonide, *J. Phys. Chem. Solids* **1**, 249 (1957).
- [16] M. Bayer, G. Ortner, O. Stern, A. Kuther, A. A. Gorbunov, A. Forchel, P. Hawrylak, S. Fafard, K. Hinzer, T. L. Reinecke, S. N. Walck, J. P. Reithmaier, F. Klopff, and F. Schäfer, Fine structure of neutral and charged excitons in self-assembled In(Ga)As/(Al)GaAs quantum dots, *Phys. Rev. B* **65**, 195315 (2002).
- [17] M. Paillard, X. Marie, P. Renucci, T. Amand, A. Jbeli, and J. M. Gérard, Spin Relaxation Quenching in Semiconductor Quantum Dots, *Phys. Rev. Lett.* **86**, 1634 (2001).
- [18] G. E. Pikus and G. L. Bir, Exchange interaction in excitons in semiconductors, *Zh. Eksp. Teor. Fiz.* **60**, 195 (1971) [*Sov. Phys. JETP* **33**, 108 (1971)].
- [19] G. L. Bir and G. E. Pikus, *Symmetry and Strain-Induced Effects in Semiconductors* (Wiley, New York, 1974).
- [20] R. I. Dzhiyev, H. M. Gibbs, E. L. Ivchenko, G. Khitrova, V. L. Korenev, M. N. Tkachuk, and B. P. Zakharchenya, Determination of interface preference by observation of linear-to-circular polarization conversion under optical orientation of excitons in type-II GaAs/AlAs superlattices, *Phys. Rev. B* **56**, 13405 (1997).
- [21] I. A. Yugova, A. Greilich, D. R. Yakovlev, A. A. Kiselev, M. Bayer, V. V. Petrov, Yu. K. Dolgikh, D. Reuter, and A. D. Wieck, Universal behavior of the electron g factor in GaAs/Al_xGa_{1-x}As quantum wells, *Phys. Rev. B* **75**, 245302 (2007).
- [22] *Optical Orientation*, edited by F. Meier and B. P. Zakharchenya (North-Holland, Amsterdam, 1984).
- [23] I. A. Merkulov, A. L. Efros, and M. Rosen, Electron spin relaxation by nuclei in semiconductor quantum dots, *Phys. Rev. B* **65**, 205309 (2002).
- [24] D. S. Smirnov, E. A. Zhukov, E. Kirstein, D. R. Yakovlev, D. Reuter, A. D. Wieck, M. Bayer, A. Greilich, and M. M. Glazov, Theory of spin inertia in singly charged quantum dots, *Phys. Rev. B* **98**, 125306 (2018).
- [25] S. Birner, T. Zibold, T. Andlauer, T. Kubis, M. Sabathil, A. Trellakis, and P. Vogl, nextnano: General purpose 3-D simulations, *IEEE Trans. Electron Devices* **9**, 2137 (2007).
- [26] P. Klenovský, P. Steindl, and D. Geffroy, Excitonic structure and pumping power dependent emission blue-shift of type-II quantum dots, *Sci. Rep.* **7**, 45568 (2017).
- [27] V. Křápek, P. Klenovský, and T. Šikola, Excitonic fine structure splitting in type-II quantum dots, *Phys. Rev. B* **92**, 195430 (2015).
- [28] T. Takagahara, Effects of dielectric confinement and electron-hole exchange interaction on excitonic states in semiconductor quantum dots, *Phys. Rev. B* **47**, 4569 (1993).